Fracture Causes of the Al-6Zn-2Cu-1Mg Alloy Transformer Bushing Cover Plate

Chao Li[1,a], Jiacheng Li[2,b], Chaohua Wang[1,c], Yongfeng Zhao[1,d], Hua Zhu[1,e], Junli Du[1, f*]

[1]Electric Power Research Institute, State Grid Henan Electric Power Company, Zhengzhou, 450052, China
[2]Henan Jiuyu Epri Electric Power Technology Co. LTD., Zhengzhou, 450052, China

[a]Chaoli0714@163.com, [b]ljc751220032@163.com
[c]326010500@qq.com, [d]yongbubian109@163.com
[e]1529157076@qq.com, [f*]dujunlizz@163.com

Abstract. Cracking occurred on the aluminum alloy sealing cover of a transformer in a 220kV substation after three years of operation. To investigate the cause, a systematic analysis was conducted on its chemical composition, macroscopic appearance, and microscopic morphology. The results revealed that the sealing cover was made of a 7xxx series aluminum alloy with a composition of Al-6Zn-2Cu-1Mg, which does not comply with the requirements of Q/GDW11717-2023, "Technical Supervision Guidelines for Metal Equipment in Power Grids" (Section 4.4.1 states that "Series 2 and Series 7 aluminum alloys should not be used"), indicating that the material was unqualified. The Al-6Zn-2Cu-1Mg aluminum alloy contains a large number of second-phase particles at the grain boundaries, which have a significant potential difference with the matrix aluminum alloy, leading to a susceptibility to intergranular corrosion. The sealing cover underwent stress corrosion cracking in a stressful and corrosive environment.

Keywords: Aluminum alloy, Transformer sealing cover plate, Corrosion, Grain boundary corrosion

1 Introduction

With the acceleration of power construction, the utilization of metallic materials in power grids has increased significantly [1-2]. Power metallic components, including transmission and transformation hardware, operating mechanisms, conductors, and towers, constitute vital parts of transmission and transformation lines, spanning the entire grid and serving functions such as connection, transmission, mechanical support, and electrical load delivery [3]. Currently, there are basically two types of materials used for electrical fittings in China: one is made of ferromagnetic materials, primarily malleable cast iron. Fittings made of this material generate eddy current losses and hysteresis losses during use, with eddy current losses being particularly severe. They have

H. Bilgin et al. (eds.), *Proceedings of the 2024 6th International Conference on Civil Engineering, Environment Resources and Energy Materials (CCESEM 2024)*, Advances in Engineering Research 253,
https://doi.org/10.2991/978-94-6463-606-2_16

drawbacks such as significant electrical energy loss, susceptibility to corona discharge, prone to damaging conductors, inconvenient installation, and high labor intensity [4-5]. Aluminum, one of the most widely used non-ferrous metals in power grids, boasts characteristics like low density, high strength, excellent electrical and thermal conductivity, good corrosion resistance, and ease of processing [6-7]. It is thus extensively applied in substation equipment line clamps, main transformer bushings, and connection terminals. However, for aluminum alloy electrical fittings used outdoors, corrosion protection is one of the critical issues that must be addressed [8-9]. Aluminum alloy components are also prone to failure, which can drastically reduce equipment efficiency and, in severe cases, lead to grid paralysis, significantly impacting grid stability and safety [10]

Electrical fittings are used in environments that, apart from typical atmospheric conditions, also encompass high-temperature and high-humidity environments, alternating dry and wet conditions, and low-temperature settings [11]. These diverse operational environments demand exceptional corrosion and aging resistance from electrical fittings. However, aluminum alloys are highly susceptible to stress corrosion, with crack nucleation and propagation occurring readily under the combined effects of stress and corrosion [12-13]. Stress corrosion is particularly destructive, as the stresses involved in stress corrosion cracking are lower than the yield strength of the material, posing a grave threat to the safety of operational products [14-15]. Especially for the 7000 series (Al-Zn-Mg-Cu) high-strength aluminum alloys, stress corrosion cracking is a critical factor affecting their service safety and stability [16]. It is reported that stress corrosion cracking accounts for over 40% of all types of corrosion occurring in aluminum alloys, causing losses of trillions of Chinese yuan annually [17].

The aluminum alloy sealing cover of a transformer in a 220kV substation, with a service life of three years, exhibited cracking. To ascertain the reason for the cracking, a comprehensive analysis was performed, including an examination of its chemical composition, macroscopic features, and microscopic structure.

2 Experimental Procedures

Photos were taken directly at the site of the failed sealing cover plate to record its morphology at the time of failure. Subsequently, ultrasonic cleaning was performed to remove dirt from its surface, followed by observation of its fracture morphology using a stereo microscope. Microstructural observations of the fracture surface were performed under the scanning electron microscope equipped with energy dispersive spectroscopy (SEM-EDS, EVO 18, Carl Zeiss, Germany).

To observe the propagation depth and path of corrosion cracks, the cover plate at the fracture site was cut horizontally, and comparisons were made between the micro-morphology and composition distribution near the fracture and those far from it. Sample for microstructure was prepared through cutting, grinding, and polishing, and subsequently etched with 5% HF (volumetric concentration) for a period of 10 seconds. Microstructural observations were performed under the scanning electron microscope equipped with energy dispersive spectroscopy (SEM-EDS, EVO 18). The surface of

the failed cover plate was thoroughly flattened using 500#, 1000#, and 2000# grit sandpapers respectively, followed by ultrasonic cleaning for the purpose of measuring the composition of the sealing cover plate. Compositional analysis of the sampled cover plate was conducted using the Oxford FOUNDRY-MASTER PRO direct-reading spectrograph.

3 Results

3.1 Macroscopic Inspection and Chemical Composition Analysis

Fig. 1 illustrates the on-site photographs and macroscopic images of the fractured sealing cover. The fracture surfaces consists of two main cracks and can be divide into four sections. Fracture Surfaces 1# and 2# intersect the bolt holes, while Fracture Surfaces 3# and 4# do not. The failed cover exhibits no apparent deformation.

Fig. 2 reveals the fracture morphologies of Fracture Surfaces 1#-4#. Fracture Surfaces 1# and 2#, delineated by the bolt holes, exhibited significant oxidation and contamination at the inner ring position of the annular cover compared to the outer ring position. This trend extended gradually from the inside of the casing upper part towards the outside of the cover, as indicated by the red arrows in Fig. 2. Fracture Surfaces 3# and 4# displayed a consistent trend, with oxidation and contamination intensifying gradually from the outer to the inner regions.

The test results of cover plate element composition are detailed in Table 1. The test results indicated a non-standard aluminum alloy with a chemical composition similar to 7XXX (Al-6Zn-2Cu-1Mg) aluminum alloy. This does not comply with the requirement in Q/GDW 11717-2017 that Series 2 and Series 7 aluminum alloys should not be used for sealing plates.

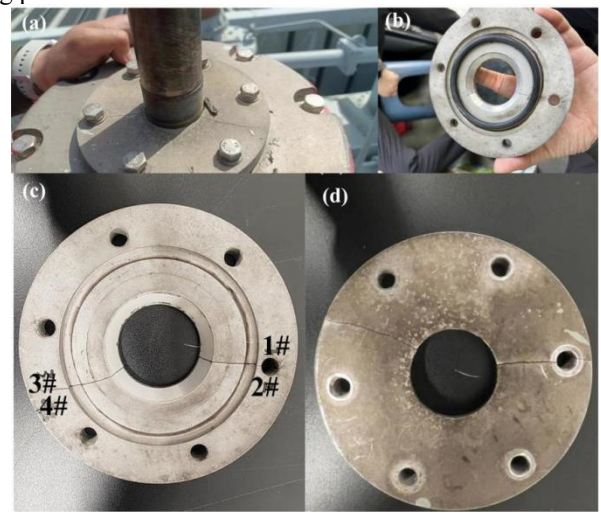

Fig. 1. Appearance of fractured sealing cover plate (a)-(b) Failure site, (b)-(d) Fracture Surfaces 1#-4#, from front and back respectively.

Fig. 2. Macroscopic morphology of fracture surface of 1#-4#.

Table 1. Test results of cover plate element composition

Composition(wt%)					
Chemical element	Zn	Mg	Cu	Mn	Fe
Measured value	6.33	1.11	1.83	0.031	0.279

3.2 Microstructure Analysis and Discussions

Fig. 3 shows the microstructural analyses of the fracture surface. The fracture surface exhibited virtually no dimples, and numerous casting defects such as microcracks and pores were visible internally, indicative of typical brittle fracture characteristics. In some areas, the fracture surface was coated with a layer of oxides, and energy dispersive spectrometry (EDS) results in Table 2 showed high concentrations of C, O, and S elements on the fracture, suggesting oxidation and contamination as the causes.

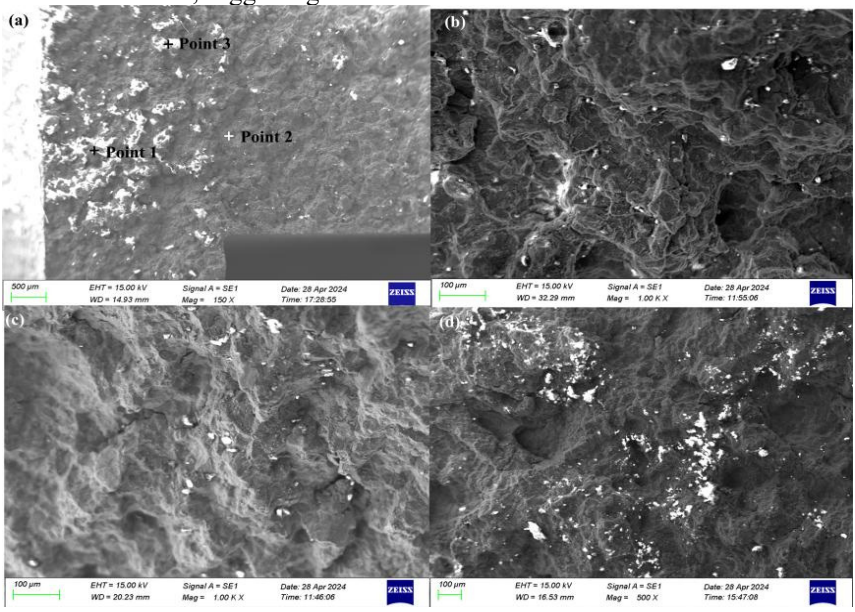

Fig. 3. (a)-(d) are the microscopic morphology of fracture surface at different locations.

Table 2. EDS results of fracture surface in Fig. 3a

Composition(wt%)					
Chemical element	C	O	Al	Zn	S
Point 1	30.11	19.74	30.82	3.66	0.61
Point 2	42.20	26.30	2.36	/	0.07

After sectioning the side of fracture surface 4# to prepare a metallographic sample, microstructural morphology and compositional analyses were conducted on the areas near the fracture. The results are presented in Figures 4-8. Fig. 4 compares the morphologies near and far from the fracture, with Fig. 4a and Fig. 4c showing the microstructures away from and near the fracture, respectively, and Fig. 4b and Fig. 4d being magnified views of Fig. 4a and Fig. 4c. From Fig. 4a-b, it is evident that the second phase is primarily distributed along the grain boundaries in a network-like pattern, with a small amount of spherical second phase present in the central regions of the crystals. No obvious microcracks are observed within the grain boundaries or interiors. Fig. 4c-d reveal that cracks propagate from the fracture along the grain boundaries into the crystal interior, as indicated by the red arrows. The distribution of cracks is more pronounced at the grain boundaries and at the interfaces with the second phase.

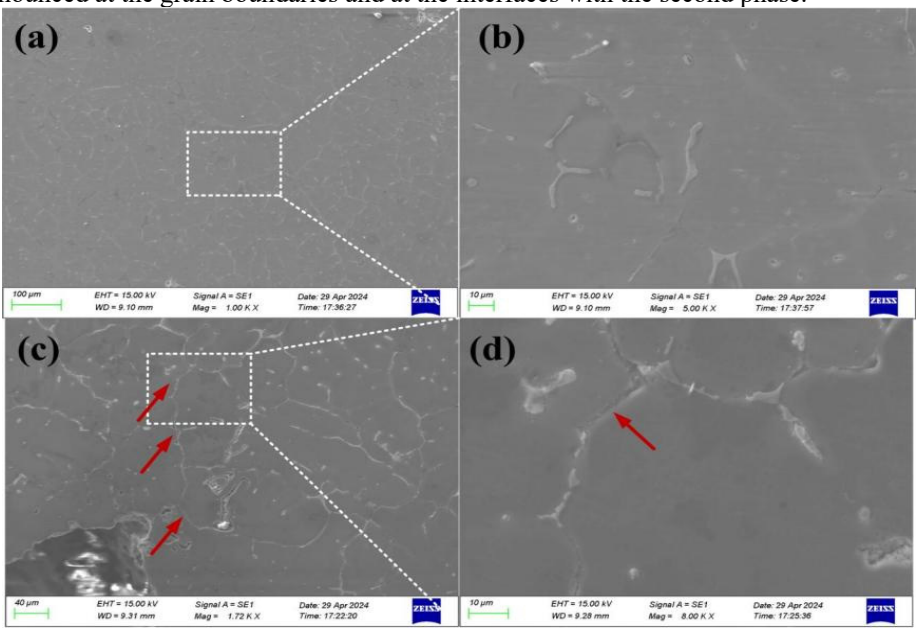

Fig. 4. Microstructure of sealing cover plate (a) away from the fracture surface and (c) near the fracture surface, (b) and (d) are the local enlarged drawing of (a) and (c).

Figs. 5 and 6 present the surface scanning energy dispersive spectroscopy (EDS) maps of Figs 4b and 6d, respectively. It is evident from these figures that the phases in

the crystalline structure away from the fracture are primarily the second phase containing Zn, Mg, and Cu, with no significant segregation of elements such as C, S, and O observed. However, scanning near the fracture in Fig. 6 reveals a notable segregation of C and O elements near grain boundaries and the second phase, located at the crack propagation sites. This demonstrates that C and O elements progressively penetrate into the sample along the cracks, resulting in significant intergranular corrosion. On one hand, the larger atomic misarrangement at grain boundaries facilitates the migration of corrosive substances such as C and O into the sample along these boundaries. On the other hand, the significant potential difference between the second phase and the aluminum matrix leads to accelerated corrosion at grain boundaries, thereby forming corrosion cracks that propagate along these boundaries.

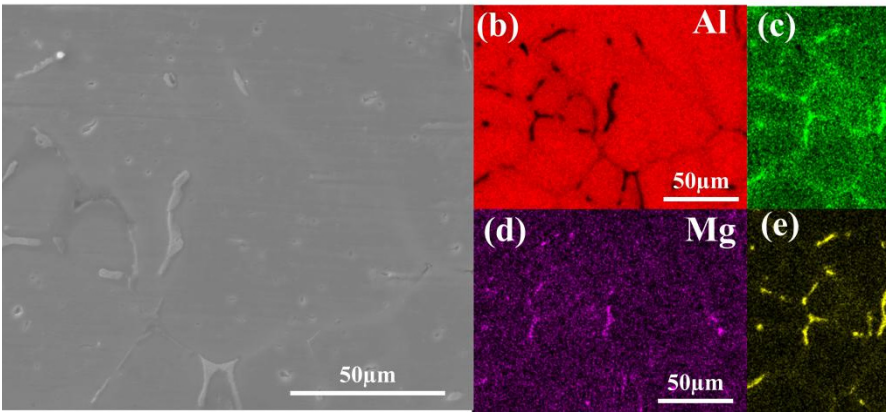

Fig. 5. (a) Mcroscopic morphology and (b)-(e) scanning energy spectrum of Al, Zn, Mg and Cu, of the surface in Fig. 4a, respectively.

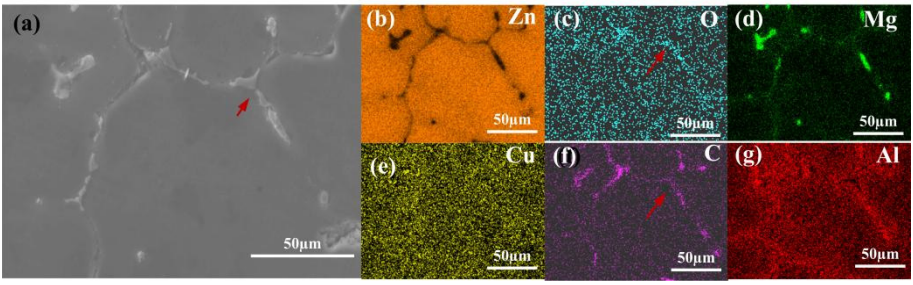

Fig. 6. (a) Microscopic morphology and (b)-(g) scanning energy spectrum of Zn, O, Mg, Cu, C and Al near the fracture surface in Fig. 4c, respectively.

Figs. 7-8 present the energy dispersive spectroscopy (EDS) maps of the microstructure near the fracture surface. Fig. 7 reveals that corrosion gradually progresses within the crystal grains besides grain boundaries, as indicated by the red arrows. The element C can be detected within the crystal grains. Fig. 8 indicates the presence of sulfur-containing corrosive substances near the fracture, in addition to oxides.

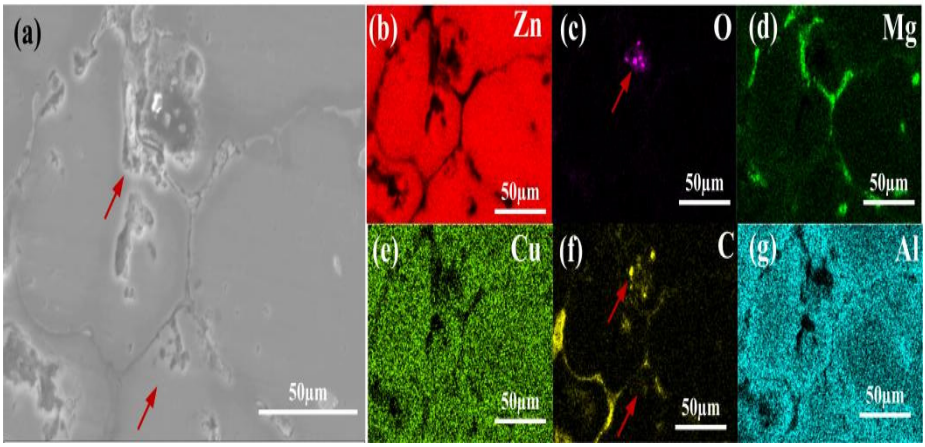

Fig. 7. (a) Microstructure and (b)-(g) scanning energy spectrum of Zn, O, Mg, Cu, C and Al near the fracture surface, respectively.

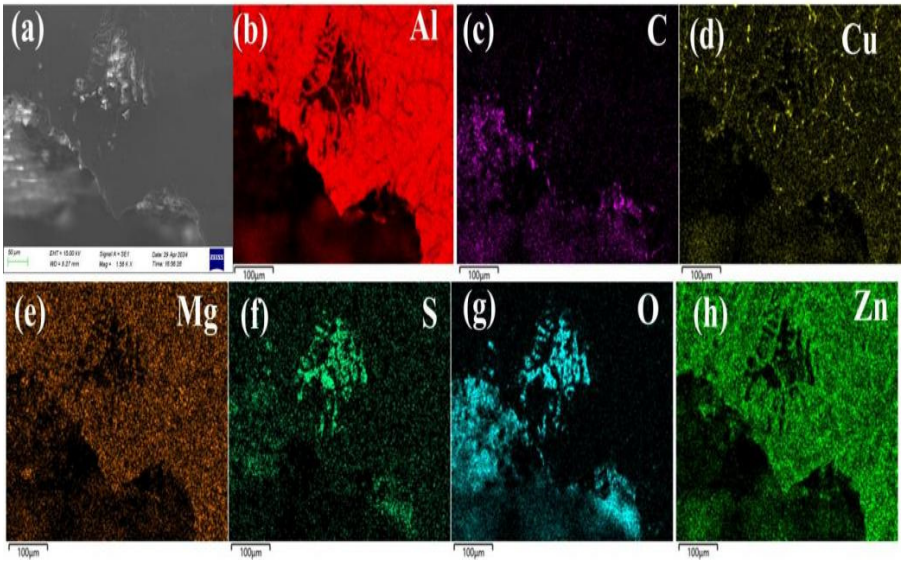

Fig. 8. (a) Microstructure and (b)-(h) scanning energy spectrum of Al, C, Cu, Mg, S, O and Zn near the fracture surface, respectively.

Fig. 9 illustrates the propagation of corrosion cracks in the vicinity of the fracture surface. It is evident from the figure that the cracks gradually extend from the fracture surface to a distance of 300-400 μm, with significant segregation of C and O elements at the crack locations.

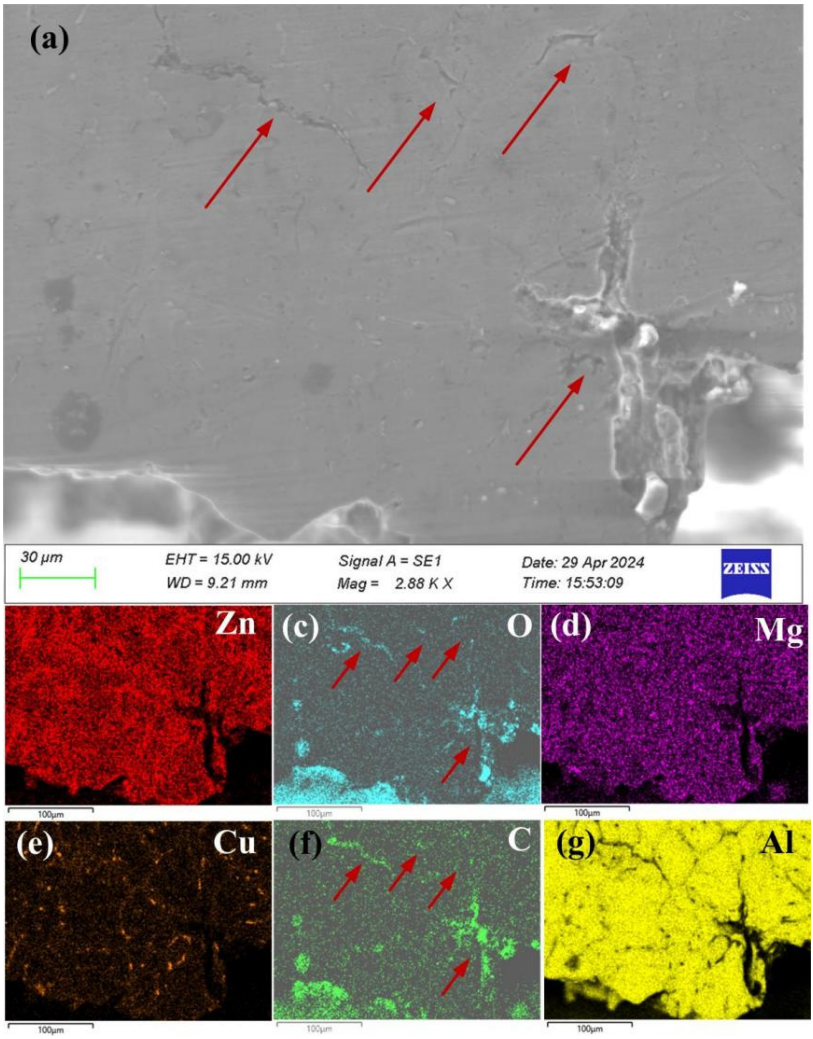

Fig. 9. (a) Microstructure and (b)-(g) scanning energy spectrum of Zn, O, Mg, Cu, C and Al near the fracture surface, respectively.

4 Conclusion

(1) The material of the sealing cover plate has been changed to Al-6Zn-2Cu-1Mg, which has a composition close to the 7xxx series aluminum alloy. However, it does not meet the requirements of Q/GDW11717-2023, Guidelines for Metal Technical Supervision of Power Grid Equipment (Section 4.4.1 states, "Aluminum alloys of series 2 and 7 shall not be used"), rendering the material.

(2) The presence of numerous second-phase particles at the grain boundaries in the Al-6Zn-2Cu-1Mg alloy results in the fracture of the sealing cover plate, which is caused

by the gradual propagation of cracks due to long-term stress corrosion at the hole location on the inner side of the plate. The networked second-phase particles at the grain boundaries exacerbate the crack propagation.

Conflict of Interest

We declare that we do not have any commercial or associative interest that represents a conflict of interest in connection with the work submitted.

Acknowledgements

Financial supports from State Grid Henan Electric Power Company science and technology Foundation (No. 52170224000U) are greatly acknowledged.

Reference

1. J. Sun, L. Jin, J. Dong, F. Wang, S. Dong, W. Ding, A.A. Luo, Towards high ductility in magnesium alloys - The role of intergranular deformation, International Journal of Plasticity 123 (2019) 121-132.
2. Li De,Yang Yan,Zhang Lijuan,et al. Electric metal devices made up of malleable cast iron with their service life upgraded by increasing pearlites[J]. Journal Liaoning Institute of Technology on Social Science,1997(1) : 28-30.
3. Niu Haijun, Fu Bin, Zhu Kuanjun, et al. Development and application of spacer and suspension clamp based on modified composites[J]. Electric Power Construction,2014,35(6) : 97-101.
4. Song Ningning, Wang Jingchao, Yan Xingjian. Development and application of a new series of energy-saving electric fittings[J]. Power System and Clean Energy,2010,26(9) : 34-37.
5. Fan Zhigang, Zhu Dechun, Wu Ming, et al. Application of 3D printing in structure design and manufacturing for network equipment[J]. Machine Building and Automation,2016,45(6) : 56-59.
6. Ji Wei,Zhang Feiyong,Meng Fandong, et al. Application research of power fittings made of high-strength aluminum alloy materials[J]. Zhejiang Electric Power,2020,39(6) : 111-114.
7. Liu Niucan, Li Junqing, Yang Mingsheng. Influence of RE and Mn additions on Fe-containing phase in Al-Si alloys [J]. Foundry Technology,2011,32(11) : 1532-1534.
8. Song Liang,Fan Peng,Zou Yongzhi,et al. Effects of microalloying on microstructure and aging behavior of Al-7%Si alloy[J]. Foundry Technology,2007(5) : 669-672.
9. Chen Zhongwei,Jie Wanqi. Effects of Mg on the microstructure and mechanical property of Al-Si-Mg casting alloys [J]. Journal of Materials Science and Engineering,2004(5) : 647-652
10. USMAN B J. Green and effective anodizing of AA 2024-T3 in methionine-sulfuric acid electrolyte[J]. Journal of The Electrochemical Society, 2022(169): 031503.
11. MOUSAVIAN S M H, TABAIAN S H. The effect of anodizing electrolyte composition on electrochemical properties of anodized magnesium. Anti-Corrosion United States:experiences and opinions of growers in three regions[J]. Hort Technology, 2019, 29(5):619- 628.

12. Huang X, Pan Q, Li B, et al. Microstructure, mechanical properties and stress corrosion cracking of Al-Zn-Mg-Zr alloy sheet with trace amount of Sc[J]. Journal of Alloys & Compounds, 2015, 650: 805-820.
13. Sun X Y, Zhang B, Lin H Q, et al. Correlations between stress corrosion cracking susceptibility and grain boundary microstructures for an Al-Zn-Mg alloy[J]. Corrosion Science, 2013, 77(12): 103-112.
14. Guyot P, Conttignies L. Precipitation kinetics, mechanical strength and electrical conductivity of Al-Zn-Mg-Cu alloy[J]. Acta Materialia, 1996, 44(10): 4161−4167.
15. Talianker M, Cina B. Retrogression and reaging and the role of dislocations in the stress corrosion of 7000-type aluminum alloys[J]. Metallurgical Transactions A, 1989, 20(10): 2087-2092.
16. Li Lanbo; Yuan Tiechui; Yuan Xiaoxing. The microstructure regulation and property enhancement of directed energy deposited Al-Zn-Mg-Cu-Si-Zr alloy with various Zr contents [J]. Materials Chemistry and Physics. 2023, 297: 127318.
17. Wang Mingtao; Wang Liwei; Yang Wendi; Liu Yuxi; Terryn Herman; Cui Zhongyu. Study on the roles of bisulfite in the stress corrosion cracking of 7050-T7451 aluminum alloy in the thin electrolyte layer environment [J]. Corrosion Science. 2023, 215:111030.